OPO OPHTHALMIC AND PHYSIOLOGICAL OPTICS
THE JOURNAL OF THE COLLEGE OF OPTOMETRISTS

Ophthal. Physiol. Opt. 2009 **29:** 357–362

Narrow angle light scatter in rabbit corneas after excimer laser surface ablation

Harilaos Ginis, Iro Pentari, Dirk de Brouwere, Dimitris Bouzoukis, Irini Naoumidi and Ioannis Pallikaris

Department of Medicine, Institute of Vision and Optics, University of Crete, Heraklion, Crete 71003, Greece

Abstract

Corneal haze following excimer laser ablation is an adverse after-effect of photorefractive keratectomy (PRK) and is associated with the development of subepithelial opacities. The present work pertains to the measurement of light scattering in rabbit corneas following excimer laser treatment; to the microscopic analysis of the light-scattering corneal structures; and to the development of a mathematical model of light propagation through the post-laser treatment cornea. Photorefractive keratectomy (PRK-6D, 6 mm optical zone) followed by standard postoperative pharmaceutical treatment was performed on rabbit eyes. Animals were examined clinically on a weekly basis and sacrificed after the tenth postoperative week. Confocal microscope image sequences were acquired immediately before animal sacrifice. After the scatter measurement, the corneas were prepared for histopathological evaluation. The subepithelial structures observed using the confocal microscope correspond to refractive index (and therefore optical path difference (OPD) variation. This OPD distribution can be approximated with a fractal surface, band-pass filtered in the Fourier domain. The angular distribution of scattered light is characterised by a narrow forward peak of the order of 0.5° full-width at half maximum (FWHM) in accordance with the sizes of the subepithelial structures (5–150 μm).The intensity of scattered light is correlated with the thickness of the subepithelial scar-tissue layer.

Keywords: corneal haze, fractal, light scatter, photorefractive keratectomy, scar tissue

Introduction

In photorefractive keratectomy (PRK) and other surface ablation procedures to compensate for refractive error, a series of UV (typically ArF Excimer 193 nm) laser pulses is delivered on the corneal surface in order to modify its curvature and adjust its dioptric power. The most common adverse effect of surface ablations is corneal haze, where a subepithelial layer of reduced transparency causes light scatter (Chang *et al*., 1996; Lohmann *et al*., 1991; Hart and Farrell, 1969). Although in most cases the patients do not report significant visual symptoms, the development of this subepithelial layer is a complication that results in a decrease in contrast sensitivity and a partial regression of the refractive error (Rajan *et al*., 2006; Meek *et al*., 2003).

The purpose of this study was to employ a single-pass optical technique to measure forward-scattered light intensity and angular distribution in excised rabbit corneas following PRK and to correlate these findings with clinically-observed haze and histopathological analysis of the specimens. The results were used to develop a mathematical model of light propagation through the hazy cornea.

Received: 2 November 2008
Revised form: 22 December 2008
Accepted: 31 December 2008

Corresponence and reprint requests to: Harilaos Ginis.
Tel.: +30 2810 394807; Fax: +30 2810 394653.
E-mail address: ginis@ivo.gr

Methods

Animal treatment

Sixteen eyes of eight pigmented adult rabbits, each rabbit weighing 2.5–3.5 kg, were studied. The animals

doi: 10.1111/j.1475-1313.2009.00649.x

were treated in accordance with the guidelines of the Association for Research and Vision in Ophthalmology Statement for the Use of Animals in Ophthalmic and Vision Research.

Before surgery (photorefractive keratectomy), the animals were anesthetized by an intramuscular injection of a mixture of xylazin hydrochloride (5 mg kg^{-1}) and ketamine hydrochloride (50 mg kg^{-1}). An eyelid speculum was introduced and two drops of topical anesthetic (sodium chloride proxymetacain, Alcaine; Alcon Laboratories Hellas, Athens, Greece) were instilled. Two minutes after topical corneal anesthesia, mechanical epithelial debridement of the central 6 mm of the cornea (previously marked with a 6 mm trephine) was performed with a brush. A myopic photoablation was then performed using a 193 nm excimer laser (Allegretto 400 Wavelight: Erlangen, Germany) operating at an average fluence of 180 mJ cm^{-2} per pulse and a repetition rate of 400 Hz. The ablation pattern delivered to all eyes was programmed for −6 diopters (D) at an optical zone of 6 mm, removing approximately 63 μm of stromal tissue in the centre of the ablation zone. Average corneal thickness prior to ablation was 384 μm (SD: 12 μm). Antibiotic ointment (Tobramycin 0.3%) was administered to all eyes four times daily until re-epithelialization was complete, in order to reduce the risk of bacterial infection.

Postoperative examinations and histopathological evaluation

All eyes were evaluated for haze development on a weekly basis, starting at week 4 postoperatively, by means of slit-lamp examination by a refractive surgeon (DM). On week 10, the animals were sacrificed and eyes were enucleated. In order to minimise edema and striae, corneas were excised along with a 2 mm scleral rim. Corneal pachymetry was also measured on a weekly basis by means of an ultrasound pachymeter (Corneo – Gage Plus™; Sonogage, Cleveland, OH, USA). Forward scattering was assessed using a single-pass device described in the following paragraph. Finally, all corneas were prepared for histologic examination (light microscopy) by trichrom staining. Histological fixation of all specimens (with glutaric aldehyde) was carried out within 5 min after enucleation. The thickness of the subepithelial scar tissue layer was measured by means of a purpose-developed MATLAB script that scaled the histological images according to the ultrasound pachymetry of each specimen. Initial evaluation of the images revealed that the thickness of the scar tissue layer was nearly uniform. Two eyes of one animal were excluded from the study due to the animal's death during the healing period and one eye was excluded due to bacterial infection leading to severe scarring. Four corneas were investigated using a confocal microscope (HRT II + cornea module; Heidelberg Engineering, Heidelberg, Germany). These four eyes were subsequently excluded from scatter analysis as they exhibited excessive levels of scatter, possibly associated with edema and/or surface defects following confocal imaging. Two eyes were excluded from the scatter measurement due to the formation of visible striae during the excision from the enucleated eye. Five corneas of rabbit eyes which had not been subjected to laser ablation also underwent scatter measurement, to serve as controls.

Optical setup for the measurement of single pass forward scatter

A purpose-built optical setup was employed for the evaluation of narrow-angle forward scattering. The setup is illustrated in *Figure 1*.

The setup involved a CCD camera (Sony XCD – X700: Sony, Tokyo, Japan) with a custom-made camera lens. The camera lens consisted of one plano-convex and one plano-concave element. The refractive surfaces of the lenses had curvatures similar to the anterior and posterior curvatures of the rabbit cornea respectively. The excised cornea occupied the space between the lenses (see enlargement in *Figure 1*). Carbomer gel 0.3% (Thilogel; Alcon) was used to facilitate optical contact between these three elements. An additional plano-convex lens (also optically coupled with carbomer gel) was used to adjust the total dioptric power of the camera

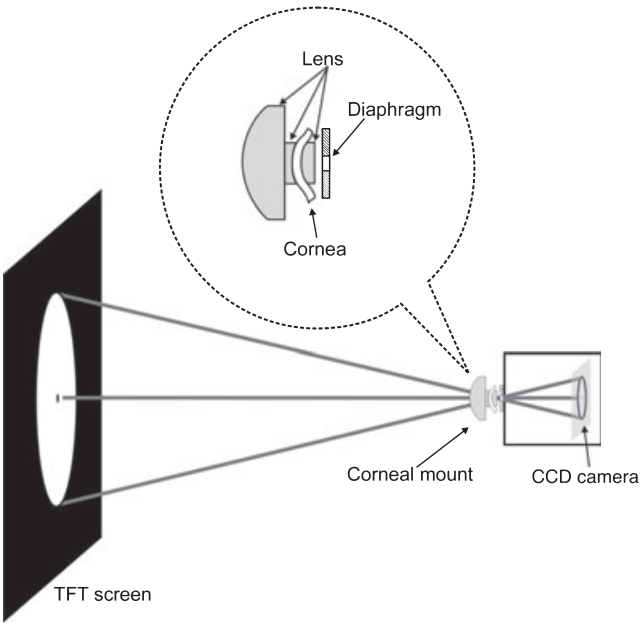

Figure 1. Optical setup for the measurement of narrow-angle forward light scatter in excised rabbit corneas. The enlarged insert shows details of the mounting of the cornea within the camera lens and the aperture stop.

lens to approximately 35 Dioptres. All lenses were aligned using a custom-made lens mount that ensured that the optical elements were properly centred. In order to minimize the impact of aberrations, a 1.2 mm diaphragm was introduced in front of the lens.

This lens was used to record images of disks featuring a central dark dot, presented on a TFT computer screen. The rationale for recording images of disks was as follows. The intensity of scattered light at angles of a few degrees on the image plane is several orders of magnitude lower than the intensity of the peak of the PSF. Therefore, it is difficult to observe and accurately quantify the amount of scattered light with respect to the maximum of the PSF in an image of a point source, as the dynamic range of the image is higher than the dynamic range of common (8 or 12-bit) digital photography. Utilizing extended sources may result in an image of lower dynamic range, with intensities of scattered light that are comparable to the maximum intensity, and can therefore be measured with higher signal-to-noise ratio and smaller relative quantization error.

Observing *Figure 2*, we can consider a disk having a small central dark dot (of practically negligible dimensions). An annular ring of angular radius ϕ and thickness $d\phi$ results in a scattered light intensity at the centre equal to $2\pi\phi \cdot PSF(\phi)d\phi$ where $PSF(\phi)$ is the value of the point Spread function of the system (including scatter) at angle φ. Therefore, considering the full disk, having an angular radius of ϑ, the cumulative intensity $I_c(\vartheta)$ at the central dark dot is:

$$I_c(\vartheta) = \int_0^{\vartheta} 2\pi\phi \cdot PSF(\phi)d\phi. \quad (1)$$

By measuring the intensity at the central dark dot for different disk radii (ϑ) experimental data can be gathered for the function $I_c(\vartheta)$ (*Figure 2*). In our method, the $PSF(\vartheta)$ is calculated by fitting a third-order spline to the experimental data for $I_c(\vartheta)$ and taking its derivative:

$$PSF(\vartheta) = \frac{1}{2\pi\vartheta}\frac{dI_c(\vartheta)}{d\vartheta}. \quad (2)$$

For each cornea, a series of 18 disks was projected and the images recorded, yielding 18 experimental values for $I_c(\vartheta)$ for angles ranging from 0.149 to 3°.

All images were corrected according to the camera's response function (determined in a separate experiment) and normalised with respect to the luminance of a full bright field of equal luminance prior to processing. The intensity of the central dark dot was measured by a purpose-developed MATLAB (The Mathworks, Inc., Natick, MA, USA) script that also identified its centroid to reduce alignment errors. The

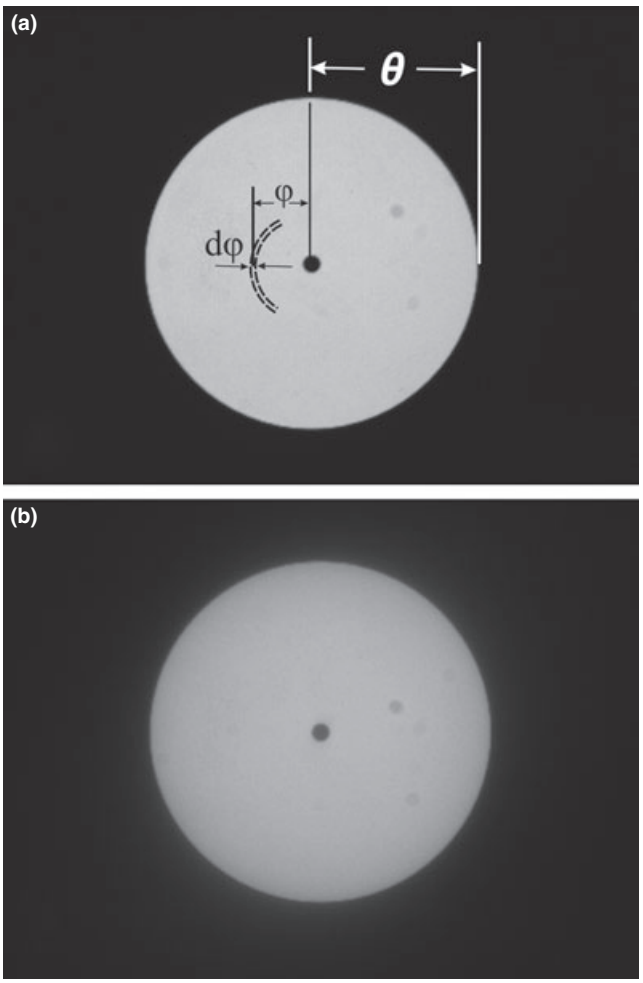

Figure 2. a: Image acquired without a cornea (space in triplet filled with clear carbomer gel) and the notation for Equations (1) and (2). b: Image acquired through a hazy cornea.

Scatter Ratio (SR) parameter was defined as the horizontal asymptote of the $I_c(\vartheta)$ function, corresponding to the total cumulative intensity of forward scatter (*Figure 3*).

Modelling scatter in the post-PRK cornea

Both *in-vivo* confocal microscopy and histology revealed that the subepithelial scar tissue consists of reflective structures that are densely packed (essentially interconnected) and moreover that the sizes of the irregularities span several orders of magnitude, ranging from the subcellular scale to a few hundreds of microns. The purpose of the proposed model is to treat light scatter as a continuous perturbation of the optical path difference across the pupil. This phase perturbation is a result of the refractive index variation of the structures observed in the sub-epithelial scar-tissue layer. In order to approximate this wavefront aberration, a fractal surface is approximated by summing N random perturbations

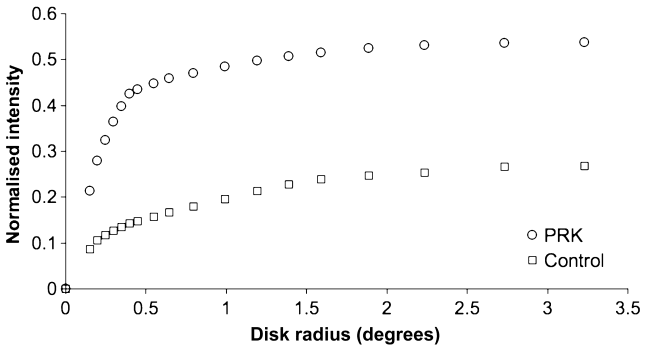

Figure 3. Cumulative intensities for two different samples. For each sample, as the disk radius is increased the normalized intensity approaches an asymptotic level which is used to define the Scatter Ratio (SR).

where each of the perturbations is a scale transformation of the previous perturbation (the spatial frequencies are doubled). The result approximates a fractal surface in the sense that in every scale it is characterised by the same statistical properties. The number of summed orders depends on the highest spatial frequency that is modelled and -of course- the desired spatial resolution of the modelled wavefront. The resulting surface can be modified in terms of its spatial characteristics by appropriate filtering in the Fourier domain. The effectiveness of this technique in modelling very high spatial frequency wavefront aberrations is demonstrated in the Results section.

Results

Figure 4 shows the correlation between the thickness of the subepithelial scar tissue layer, as measured histologically, and the Scatter Ratio. Scatter measurements of five unablated rabbit corneas are also plotted for comparison.

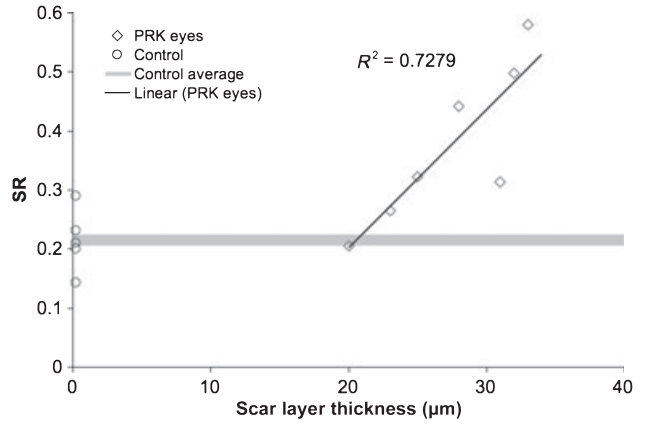

Figure 4. Scatter Ratio (SR) as a function of scar layer thickness for control and post-PRK corneas. The black line is a regression fit to the post-PRK data.

Evidently there is significant scatter even from the eyes which have not been subjected to excimer laser ablation. The data of *Figure 4* indicate that our method of excision of the cornea and mounting on the glass triplet results in a baseline light scatter of the order of 21% (SR = 0.211).

Figure 5 shows the calculated point-spread functions for an intact and a post-PRK cornea.

It can be seen that the intact cornea scatters more light at wide angles whereas the post PRK cornea is characterised by a narrower distribution. It is reasonable to assume that scatter in the intact cornea originates from keratocytes and the mild edema caused by the surgical manipulations during excision. In addition to these factors, the post-PRK cornea has a scar-tissue layer and a relatively rough epithelial-stromal interface. These features are both characterised by irregularities of the scale of several tens to hundreds of microns, which are likely to contribute to narrow-angle forward light scatter (0–0.5°).

The thickness of the scar tissue layer was not correlated with changes in corneal pachymetry. Difference in pachymetry was calculated as the difference between the 4th and the 10th week, while thickness of the scar tissue layer was estimated by computer processing of the histology images, as described in the Methods section. The lack of correlation suggests that the scar tissue layer is not solely newly-formed collagen but possibly involves existing collagen that progressively loses its natural uniformity in terms of organization. Although the mechanism is not clear, it is reasonable to expect that severed (but not ablated) collagen fibers may be displaced by the newly-formed collagen, thus forming structures of variable density.

Figure 6 shows the suitability of a fractal image for the simulation of the scar tissue layer.

The generalised pupil function for the simulated PSF in *Figure 6* was constructed by taking into account not only the optical path difference but also the reflectivity of the structures modulating the transmitted intensity.

This model can be expanded to incorporate aberrations as well as scatter. In this unified view of the PSF, the scatter ratio (SR) can be defined in a manner similar to that of the Strehl ratio, where the reduction of the peak of the PSF is associated with scatter. It must be noted that this definition of the SR is equivalent to the definition based on the asymptote of the cumulative intensity for large angles, as given in the Methods section.

Discussion

Our results suggest that the subepithelial scar-tissue layer is the primary factor contributing to the increased corneal scatter which follows surface ablations. This is

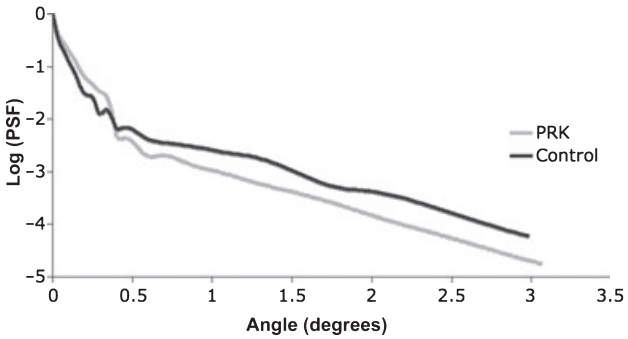

Figure 5. Calculated point spread functions (PSF) for a control and post-PRK cornea (normalised at their peak intensity).

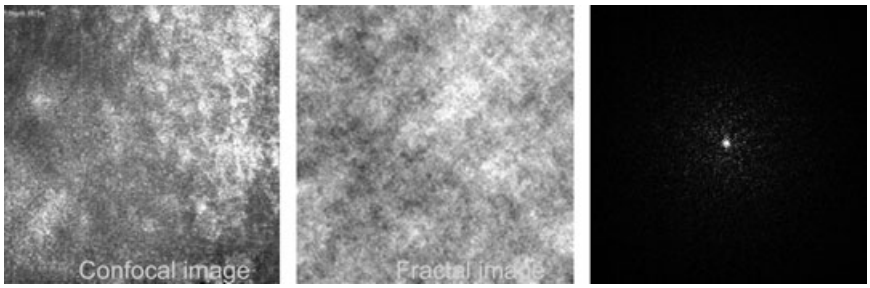

Figure 6. Left: Confocal microscope image. Middle: Fractal image of similar spatial characteristics. Reflectivity (variation of the refractive index) can be directly expressed as optical path difference. Right: PSF of a system; the wavefront aberration corresponds to that in the middle image. (In this example, Peak to Valley wavefront aberration = 0.2μm Scattering Ratio = 0.34).

in accordance with our previous finding using a less sensitive technique to measure the PSF (De Brouwere *et al*., 2008). The angular distribution of scatter in hazy corneas is narrower than that of healthy corneas, suggesting that the large structures seen in the scar tissue layer contribute strongly to scatter. The irregularities in the scar tissue layer (in this study 20–30μm deep) are extracellular reflective structures (Moller-Pedersen, 2004; Meek *et al*., 2003; Perez-Gomez and Efron, 2003; Frueh *et al*., 1998; Böhnke *et al*., 1998) characteristic of scar tissue. The hypothesis that this layer is the main cause of scatter is further supported by the strong correlation of its thickness with the calculated Scatter Ratio. Our ultrasound pachymetry measurements did not reveal a correlation between changes in corneal thickness during the healing period and the thickness of the scar tissue layer. This finding suggests that the scar tissue is not only newly formed collagen but possibly involves existing collagen that is progressively losing its geometrical organisation during the healing period.

The spatial characteristics of the scar tissue layer are closely related to the angular distribution of light scatter. Although the morphological comparison of the scar tissue layer in rabbits and the corresponding layer in humans was beyond the scope of the present study, there appears to be a similarity in the appearance of these layers in confocal microscopy. Given that essentially the angular distribution of scattered light is related to the 2-dimensional Fourier transform of the confocal image, the present study may serve as the basis for the connection between confocal microscopy and estimation of forward light scatter intensity and distribution.

Our analysis was based on measurements made 10 weeks after the laser treatment, since it has been reported (Perez-Gomez and Efron, 2003) that at about this post-operative time interval the effect of the healing response reaches a maximum, and the highest haze grade (Moller-Pedersen, 2000) is observed. In the longer term, haze decreases rapidly between 3 and 6 months and shows a further slower decrease up to 1 year (Frueh *et al*., 1998). Although usually no significant backscattered haze is observed one year after surgery, collagen irregularities and the subepithelial scar tissue that remain in the stroma might give rise to a steady state of increased forward scatter. Despite the reduction of backward scatter, it must be considered that forward scattered light is far more intense than backscattered light, and therefore that PRK patients may experience the effects of increased straylight even when the cornea appears effectively clear in the clinical examination (Böhnke *et al*., 1998).

Although psychophysical methods (Franssen *et al*., 2006) can be used for the evaluation of straylight after refractive procedures (Beerthuizen *et al*., 2007) the methodology presented may prove useful for the evaluation of corneal transparency in animal models. It may

be applied to the initial evaluation of different surgical modalities and postoperative pharmaceutical treatment schemes, to assess their effectiveness in the prevention of postoperative haze. Moreover, understanding the spatial characteristics of the scatterers and the corresponding angular distribution of scattered light may improve our understanding of the impact of haze on visual function.

References

Beerthuizen, J. J., Franssen, L., Landesz, M. and van den Berg, T. J. (2007) Straylight values 1 month after laser in situ keratomileusis and photorefractive keratectomy. *J. Cataract Refract. Surg.* **33,** 779–783.

Böhnke, M., Thaer, A. and Schipper, I. (1998) Confocal microscopy reveals persisting stromal changes after myopic photorefractive keratectomy in zero haze corneas. *Br. J. Ophthalmol.* **82,** 1393–1400.

Chang, S. S., Maurice, D. M. and Ramirez-Florez, S. (1996) Quantitative measurement of corneal haze after myopic PRK. *J. Refract. Surg.* **12,** 412–416.

De Brouwere, D., Ginis, H., Kymionis, G., Naoumidi, I. and Pallikaris, I. (2008) Forward scattering properties of corneal haze. *Optom. Vis. Sci.* **85,** 843–848.

Franssen, L., Coppens, J. E. and van den Berg, T.J. (2006) Compensation comparison method for assessment of retinal straylight. *Invest. Ophthalmol. Vis. Sci.* **47,** 768–776.

Frueh, B. E., Cadez, R. and Böhnke, M. (1998) In vivo confocal microscopy after photorefractive keratectomy in humans. A prospective, long-term study. *Arch. Ophthalmol.* **116,** 1425–1431.

Hart, R. W. and Farrell, R. A. (1969) Light Scattering in the Cornea. *J. Opt. Soc. Am.* **59,** 766–775.

Lohmann, C. P., Gartry, D. S., Muir, M. K., Timberlake, G. T., Fitzke, F. W. and Marshall, J. (1991) Corneal haze after excimer laser refractive surgery: objective measurements and functional implications. *Eur. J. Ophthalmol.* **1,** 173–180.

Meek, K. M., Leonard, D. W., Connon, C. J, Dennis, S. and Khan, S. (2003) Transparency, swelling and scarring in the corneal stroma. *Eye* **17,** 927–936.

Moller-Pedersen, T. (2000) Stromal wound healing explains refractive instability and haze development after photorefractive keratectomy. *Ophthalmology* **107,** 1235–1245.

Moller-Pedersen, T. (2004) Keratocyte reflectivity and corneal haze. *Exp. Eye Res.* **78,** 553–560.

Perez-Gomez, I. and Efron, N. (2003) Change to corneal morphology after refractive surgery as viewed with a confocal microscope. *Opt. Vis. Sci.* **80,** 690–697.

Rajan, M. S., O'Brart, D., Jaycock, P. and Marshall, J. (2006) Effects of ablation diameter on long-term refractive stability and corneal transparency after photorefractive keratectomy. *Ophthalmology* **113,** 1798–1806.